IEICE TRANS. FUNDAMENTALS, VOL.E87–A, NO.10 OCTOBER 2004

PAPER Special Section on Wide Band Systems

On the Code Synchronization of PPM/OPPM Fiber-Optic CDMA Systems

Anh T. PHAM[†a)], ***Student Member and*** **Hiroyuki YASHIMA**[††], ***Member***

SUMMARY This paper proposes and theoretically evaluates two different schemes of code acquisition for pulse-position modulation (PPM) and overlapping PPM (OPPM) fiber-optic code-division multiple-access (CDMA) systems, namely threshold-based and demodulator-based code acquisition. Single-dwell detector and serial-search algorithm are employed for both schemes. Theoretical analysis is carried out for shot-noise-limited photon-counting receiver. Discussions upon effects of various parameter settings on the performance of code acquisition for PPM/OPPM fiber-optic CDMA systems, such as index of overlap, PPM/OPPM multiplicity, average photon counts per information nat, and darkcurrents, are presented. It is shown that when the threshold is properly selected, the threshold-based code acquisition system offers better performance, in terms of mean number of training frames, than the demodulator-based one.

key words: *fiber-optic CDMA, PPM, OPPM, optical orthogonal codes, code acquisition and synchronization, serial-search algorithm, multiple-access interference, shot-noise-limited receiver*

1. Introduction

With the explosive growth of on-demand and multimedia services, high-speed connections are nowadays required up to last-mile access networks. The fiber-optic, with its clear advantages over metallic wire, has been considered an inevitable choice for wired access networks. In order to save cost and to make use of vast bandwidth provided by fiber-optic, optical multiplexing methods have been considered for multiple-access, such as wavelength-division (WDMA), time-division (TDMA) and most recently code-division (CDMA).

In the TDMA system, the total throughput is limited by the product of number of users and their data rates. Moreover, management and coordination regarding slot assignment cause significant latency penalties [1]. The WDMA system allows user to transmit at its peak speed since separate wavelengths are used, it however wastes significant bandwidth to implement complicated schemes for channel control and collision detection to secure a dynamic multiple-user set [2]. Meanwhile, in fiber-optic CDMA systems, neither time nor frequency management is required. Moreover, asynchronous access for a dynamic and possible large number of users, much larger than number of wavelengths, could be provided with inherent security by fiber-optic CDMA. In the access network environment, flexible, less-maintenance system for a dynamic and large multiple-user set is preferable, fiber-optic CDMA is therefore considered better choice in comparison with traditional TDMA and WDMA.

Several approaches to fiber-optic CDMA have been introduced, of which time-domain encoding system is the most attractive one because of its simplicity and compatibility to the present intensity-modulation/direct-detection (IM/DD) optical systems [3]. In time-domain encoding fiber-optic CDMA systems, transmitted signals are formed by imprinting an unique spreading sequence onto optical pulses. At the receiver end, transmitted information is recovered by correlating received signal with the local replica of the desired user's spreading sequence. Code synchronization between transmitter and receiver is strictly required so as peak auto-correlation value could be obtained. Generally, code synchronization can be performed in two steps. First, in initial synchronization, or acquisition, the coarse alignment between the incoming spreading sequence and its local replica within a small fraction, e.g. half chip duration, is located. Once the coarse alignment is found, the system enters lock mode where the fine alignment is achieved and maintained by tracking system [14]. Of these two, code acquisition is the most challenging task.

Our present research focuses on code acquisition methods for time-domain encoding fiber-optic CDMA systems. Particularly in this paper, we work on code acquisition systems using single-dwell detector and serial-search algorithm for PPM and OPPM fiber-optic CDMA systems. The PPM fiber-optic CDMA is considered as a special case of OPPM when the index of overlap equals one.

1.1 Related Works

Code synchronization for wireless CDMA communications has been heavily studied [14]. Serial-search algorithm has been proposed and intensively studied by Polydoros and Weber [13]. It has been shown that serial-search algorithm is better than other search methods, such as maximum-likehood and sequential estimation, because it offers the trade-off of simplicity and performance in the low signal-to-noise environment [14].

In the domain of fiber-optic CDMA, particularly time-domain encoding fiber-optic CDMA, several works has been documented so far. First, Yang [4] showed degradation in the system performance when synchronization is not ideal,

Manuscript received February 15, 2004.
Manuscript revised May 15, 2004.
Final manuscript received June 22, 2004.

[†]The author is with Department of Information and Computer Sciences, Saitama University, Saitama-shi, 338-8570 Japan.
[††]The author is with Department of Management Science, Tokyo University of Science, Tokyo, 162-8601 Japan.
a) E-mail: pham@sie.ics.saitama-u.ac.jp

and proposed a simple synchronization method for on-off keying (OOK) fiber-optic CDMA systems. Mustapha and Ormonroyd introduced serial-search synchronizer with single and dual-threshold sequential detector [5] and [6]. Later, Keshavarzian and Salehi investigated serial-search synchronizer for fixed single-dwell detector [7]. Our research group also proposed fixed multiple-dwell detector [8], which offers better performance in comparison with the single-dwell one. Nevertheless, all of these works are devoted to OOK fiber-optic CDMA systems. Regarding PPM/OPPM fiber-optic CDMA systems, there have been works highlighting the importance of code synchronization [9] and [10]; however, to our knowledge, no investigation on code acquisition has been appeared in literature so far.

1.2 Main Contributions

First, this work proposes and theoretically analyzes code acquisition for PPM/OPPM fiber-optic CDMA systems. Two schemes of code acquisition are proposed, namely threshold-based and demodulator-based code acquisition. Second, we obtain the optimal threshold values for threshold-based code acquisition for different parameter settings. Moreover, we find out that when threshold value is properly selected, threshold-based code acquisition system offers better performance than that of demodulator-based one. Finally, we provides an insightful discussions and investigation of the effects of various system parameters, such as index of overlap, PPM/OPPM multiplicity, spreading sequence weight, photon counts per information nat, and dark-currents on the performance of both proposed code acquisition schemes.

2. System Models

PPM/OPPM are the optical block encoding techniques, by which an optical pulse is placed in one of M timeslots to represent the data block. Data word is determined by the location of the pulse in the frame. In PPM, timeslots are completely separated while overlapping is allowed in OPPM. In comparison with OOK modulation, PPM/OPPM are easier for implementation because they do not require any information about signal and noise power.

Fiber-optic CDMA systems employing PPM and OPPM were proposed in [11] and [12], respectively. It has been shown that the system employing PPM has better power efficiency in comparison with the one with OOK, it is however no advantage in using PPM under fixed throughput and chip pulsewidth [11]. Alternatively, as overlapping between timeslots is allowed in OPPM signals, OPPM could improve the system's throughput while keeping chip pulsewidth unchanged [12].

The principle diagram of PPM/OPPM fiber-optic CDMA system with code acquisition system is shown in Fig. 1. From data source, M-ary data symbols are generated. These data symbols are used to modulate the position of laser pulses to form the PPM/OPPM signals. The

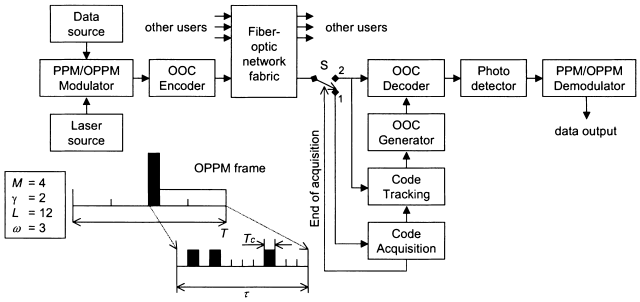

Fig. 1 Principle diagram of a PPM/OPPM fiber-optic CDMA system with code acquisition.

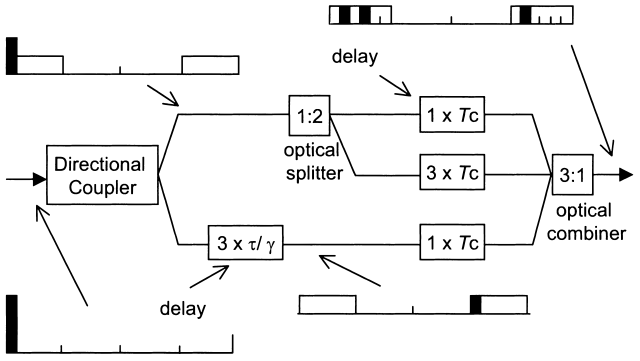

Fig. 2 Sample of encoder for wrapped OPPM fiber-optic CDMA signal; $M = 4, \gamma = 2, L = 12$, and $\omega = 3$, the spreading sequence {010000010100} is used.

PPM/OPPM fiber-optic CDMA signals are formed by imprinting a spreading sequence, with good correlation properties, onto the PPM/OPPM signals. An example of OPPM fiber-optic CDMA signal format is also depicted in Fig. 1 with multiplicity $M = 4$, and index of overlap $\gamma = 2$; the spreading sequence has length $L = 12$ and weight $\omega = 3$; T denotes the frame width. The allowable spreading interval of each OPPM[†] timeslot is τ, and T_c denotes the width of a OPPM fiber-optic CDMA chip pulse. The relation between these parameters is as follows.

$$T = M\frac{\tau}{\gamma} = M\frac{LT_c}{\gamma}. \tag{1}$$

It is important to note that the cyclic shifts are allowed for forming OPPM signals. It means when pulses are appeared in some last slots where the overlapping with the next frame might happen, the spreading interval is wrapped to the beginning of the OPPM frame. A special technique, as depicted in Fig. 2, is used for OOC encoder so that wrapped signal could be formed [12].

At the receiving end, before any data transmission between the receiver and the transmitter, switch S is at position 1 so that the acquisition process can be performed. Once the acquisition state is achieved, a control signal that indicates the end of acquisition is generated by the acquisition system to switch S from position 1 to 2. From here system

[†]Note that when $\gamma = 1$, OPPM becomes PPM, from here we therefore consider PPM as a special case of OPPM.

enters lock mode, where the fine alignment is achieved and maintained by a tracking loop, e.g. delay-locked loop or tau-dither loop.

To perform the acquisition process, a training pattern of OPPM frames that always have signal in a specific slot, e.g. in the first slot, is sent by the transmitter to the receiver. At the OOC decoder, which is fabricated of parallel optical tapped delay-lines [3], the local replica of spreading sequence at some chip position, or "cell" as it is usually called in serial-search parlance [14], is correlated with the received signal plus noise. The correlated signal is then passed to a photodetector, where optical signal is converted into electrical signal. The cell correctness is then tested. If the test result is a "hit," i.e. the system initially determines that the correct cell is being observed, the system will go to verification mode to verify that test result; otherwise it shifts the local spreading sequence replica to the next cell for a new test. The acquisition state is declared only when a "hit" test result is successfully verified.

Basically, observed cell's correctness can be tested by using an OPPM demodulator. The diagram of the code acquisition system using OPPM demodulator, or demodulator-based code acquisition, is described in Fig. 3(a). The cell correctness is tested by comparing the photon counts over the M timeslots of OPPM frame. If the first slot has the greatest photon counts, test result is a "hit," otherwise it is a "miss." The major advantage of using the demodulator-based code acquisition is that no information about signal and noise power is required. We also propose another scheme to test a cell's correctness by using a threshold, the diagram of threshold-based code acquisition system is described in Fig. 3(b). With this scheme, the correctness of a cell is decided upon whether photon counts over the first slot is higher than a preset threshold level. The major issue in the threshold-based code acquisition is consequently the determination of optimal threshold levels.

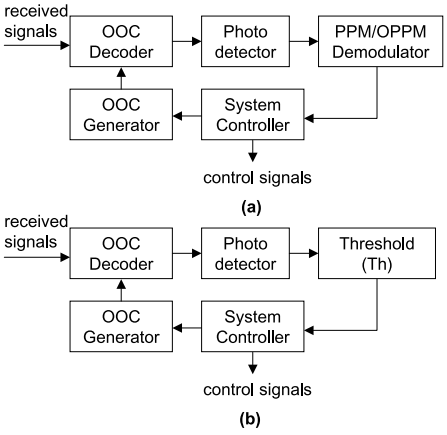

Fig. 3 (a) Demodulator-based code acquisition and (b) Threshold-based code acquisition.

3. Theoretical Analysis

In this section, we theoretically analyze two above-mentioned code acquisition schemes. Multiple access interference (MAI), darkcurrents and shot-noise (shot-noise-limited photon-counting receiver is assumed) are taken into consideration. Optimal optical orthogonal codes (OOCs), whose off-peak auto-correlation and cross-correlation are bounded by only one [3], are assumed for the spreading sequence. The comparison between two schemes will be made in averaging approach, by which the distributions of users' delay as well as of interfering pulse chips are considered as random variables.

3.1 SS/SD Code Acquisition and Markov Chain Model

In investigation of code acquisition systems, acquisition time, i.e. the time required to complete the acquisition operation, is the most important parameter. Especially in fiber-optic CDMA systems, because spreading sequences are usually exceedingly long, the task to locate the correct cell is thus very challenging. The exceeding acquisition time results in large overhead that is unacceptable in the practical communications. Noting that as acquisition time is a random variable, which is difficult to quantify, its mean value is usually used instead.

In the single-dwell serial-search (SD/SS) code acquisition system, all cells are serially tested until the correct one is found; and a single fixed interval, called dwell time, is required to check the incorrectness of a cell. In this paper, we assume the correct cell is the one corresponding to a coarse alignment of within a half code chip, and the dwell time equals to an interval of OPPM frame. We also assume that there is one test per spreading sequence chip, i.e. the uncertainty region in acquisition consists of L cells (with L is spreading sequence length). With these assumptions, the acquisition time can be represented by the required number of training frames, which is denoted as N_{ACQ}. It is important to note that due to the nature of serial-search algorithm, the mean number of training frames, which is equivalent to a half spreading sequence length, could be achieved; this is considered as the optimal performance of fiber-optic CDMA systems using serial-search algorithm.

The flow graph representing L-state Markov chain transition diagram of the SD/SS acquisition system can be illustrated in part in Fig. 4. The acquisition state (ACQ) can be directly reached only from the L-th state, whereas the false alarm state can be directly reached from any of remaining $L-1$ states. Let $U(z)$ be the moment generating function (MGF) for the flow graph, the mean number of training frames can be obtained by [14].

$$E\{N_{ACQ}\} = \left.\frac{dU(z)}{dz}\right|_{z=1}. \tag{2}$$

Assuming that there is no prior information about the correct cell, i.e. the probability to begin acquisition process

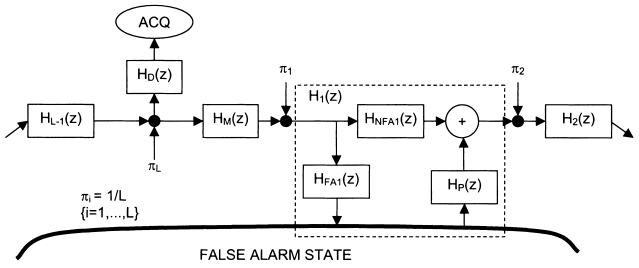

Fig. 4 Part of state diagram of SD/SS code acquisition system.

at any cell is the same and thus equals to $1/L$, the MDF $U(z)$, with help of flow graph reduction technique, can be expressed as [14]

$$U(z) = \frac{1}{L}\frac{H_D(z)}{1 - H_M(z)H_1(z)\ldots H_{L-1}(z)}\sum_{i=1}^{L}\prod_{j=i}^{L-1}H_j(z), \tag{3}$$

where,

- $H_D(z) = P_D z$ is the gain of branch from L-th cell to ACQ, here P_D is probability of detection;
- $H_M(z) = (1-P_D)z$ is the gain of branch connecting L-th to 1st cell;
- $H_i(z) = H_{NFAi}(z) + H_{FAi}(z)H_P(z)$ is the gain for connecting from i-th to $(i+1)$-th cell;
- $H_{FAi}(z) = P_{FAi}z$ is gain for false alarm occurrence in i-th cell, with P_{FAi} is probability of false alarm at i-th cell;
- $H_{NFAi}(z) = (1 - P_{FAi})z$ is the gain from i-th to $(i+1)$-th cell without false alarm;
- and, $H_P(z) = z^K$ is gain for penalty after false alarm occurrence, here K is the penalty caused by false alarm in the verification.

From (2) and (3), after simplification the mean number of training frames can be obtained as

$$E\{N_{ACQ}\} = \frac{L}{P_D} - \frac{L-1}{2} + \frac{K(1-P_D)}{P_D}\sum_{i=1}^{L-1}P_{FAi} + \frac{K}{L}\sum_{i=1}^{L-1}iP_{FAi}. \tag{4}$$

3.2 Probabilities of False Alarm and Detection

In this section, we derive the probabilities of false alarm and detection for OPPM demodulator-based and threshold-based SD/SS code acquisition. Frame synchronous for all users is assumed. This assumption, while make mathematical analysis simpler, does not affect much to the final result [12].

3.2.1 Demodulator-based Code Acquisition System

In the demodulator-based code acquisition system, "hit" is the event when the photon counts over the first slot is the highest. Let P_c be the probability of "hit," P_c can be given as

$$\begin{aligned} P_c &\equiv P_r\{\bigcap_{m=1}^{M-1}(Y_0 \geq Y_m)|b_0 = 0\} \\ &\leq \prod_{m=1}^{M-1}P_r\{Y_0 \geq Y_m|b_0 = 0\} \\ &\leq \prod_{m=1}^{M-1}P_r\{Y_0 \geq Y_m|\nu_m = 0, b_0 = 0\} \\ &\leq P_r\{Y_0 \geq Y_1|, \nu_1 = 0, b_0 = 0\}^{M-1}, \end{aligned} \tag{5}$$

where, Y_m denotes the photon counts over m-th slot of training frame of the evaluated user, $b_0 = 0$ indicates that there is always signal in the first slot of OPPM frames, ν_m denotes the number of pulses that causes self-interference to slot m-th due to the signal sent in slot 0 by the desired user. As the optimal OOC was assumed, ν_m could be either "0" or "1"; and when $\nu_m = 0$, there will be less optical power in Y_m. This validates the second transformation in inequality (5). The first transformation can be verified using Fig. 5 that shows the upper and lower bounds of BER in OPPM CDMA systems derived in [12] and the BER's lower bound due to (5).

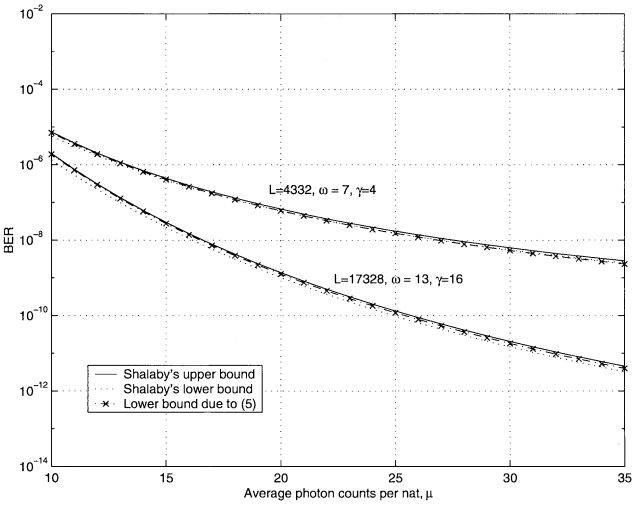

Fig. 5 OPPM fiber-optic CDMA system's BER upper and lower bounds as [12], and BER lower bound due to inequality (5). Number of users $N = 50$, OPPM multiplicity $M = 32$, darkcurrents are neglected.

Denote l and k as the number of interfering optical pulses in the first and second slots, $P_c(l)$ could be derived as

$$\begin{aligned} P_c(l) &\leq P_r\{Y_0 \geq Y_1|, \nu_1 = 0, b_0 = 0, l\}^{M-1} \\ &= \sum_{k=0}^{N-1-l}P_r\{k|l\} \\ &\quad P_r\{Y_0 \geq Y_1|, \nu_1 = 0, b_0 = 0, l, k\}^{M-1}, \end{aligned} \tag{6}$$

where,

$$P_r\{k|l\} = \binom{N-1-l}{k}q^k(1-q)^{N-1-l-k}, \tag{7}$$

here, $q = \gamma\omega^2/(M-1)L$ [12]. And

$$P_r\{Y_0 \geq Y_1|, \nu_1 = 0, b_0 = 0, l, k\} = \sum_{j=0}^{\infty} \mathrm{Pos}(j, E[Y_0]) \sum_{i=0}^{j-1} \mathrm{Pos}(i, E[Y_1]), \quad (8)$$

where,

$$E[Y_1|\nu_1 = 0, b_0 = 0, l, k] = k\lambda_s + \lambda_d, \quad (9)$$

$$E[Y_0|\nu_1 = 0, b_0 = 0, l, k] = (I_0 + l)\lambda_s + \lambda_d, \quad (10)$$

$$\mathrm{Pos}(x, y) = e^{-y}\frac{y^x}{x!}. \quad (11)$$

here, λ_s and λ_d are the average photon counts generated from a code chip and darkcurrents, respectively. I_0 represents the number of optical chip pulses from the desired signal to the first slot. Noting that the correct cell is corresponding to a coarse alignment of within a half code chip, I_0 then can be given by

$$I_0 = \begin{cases} \omega/2 & \text{the correct cell is observed} \\ 1 & \text{incorrect cell is observed} \end{cases} \quad (12)$$

here, ω is OOC's code weight. P_D and P_{FA} are P_c when the correct cell or an incorrect cell is observed, respectively. It is seen that both P_D and P_{FAi} are conditional on l_i, the number of interfering chips within the first slot of OPPM frame when i-th cell is observed. Moreover, l_i depends on the distribution of users' delays as well as distribution of code chips in each user, which, in the most general case, could be considered random variables. The $E\{N_{ACQ}\}$ thus could be computed with averaged P_D and P_{FAi}, from (4) we have

$$E_{Ave}\{N_{ACQ}\} = E\left\{\frac{1}{P_D}\right\}L - \frac{L-1}{2} + K\sum_{i=1}^{L-1} E\left\{\frac{P_{FAi}}{P_D}\right\} - K\sum_{i=1}^{L-1} E\{P_{FAi}\} + \frac{K}{L}\sum_{i=1}^{L-1} iE\{P_{FAi}\}, \quad (13)$$

Under the assumption that users' delays have uniform distribution, l_i could be obtained as a binomial random variable [12], which is expressed as

$$P_r\{l\} = \binom{N-1}{l} p^k (1-p)^{N-1-l}, \quad (14)$$

where, $p = \gamma\omega^2/ML$ [12]. Furthermore, assuming l_is are mutually independent we have

$$E\left\{\frac{P_{FAi}}{P_D}\right\} = E\{P_{FAi}\}E\left\{\frac{1}{P_D}\right\}. \quad (15)$$

Therefore, we can have the average of $E\{P_{FAi}\}$ and $E\{\frac{1}{P_D}\}$ over l_i as follow.

$$E\{P_{FAi}\} \equiv E_{l_i}\{P_{FA}|l = l_i\} = \sum_{l=0}^{N-1} P_r\{l\} \cdot \sum_{k=0}^{N-1-l} P_r\{k|l\}P_r\{Y_0 \geq Y_1|b_0 = 0, k, l\}^{M-1}, \quad (16)$$

$$E\left\{\frac{1}{P_D}\right\} \equiv E\left\{\frac{1}{P_D|l}\right\} = \sum_{l=0}^{N-1} P_r\{l\}\frac{1}{\sum_{k=0}^{N-1-l} P_r\{k|l\}P_r\{Y_0 \geq Y_1|b_0 = 0, k, l\}^{M-1}}. \quad (17)$$

Employing (16), (17) to (13), we can finally compute the average of $E\{N_{ACQ}\}$ for the OPPM demodulator-based code acquisition system.

3.2.2 Threshold-based Code Acquisition System

The threshold-based code acquisition has been proposed for OOK fiber-optic CDMA systems [7]. Though the similar structure is used, the threshold-based code acquisition is employed for different systems in this paper, i.e. PPM/OPPM fiber-optic CDMA systems. Accordingly, new analysis on effects of PPM/OPPM's special parameters, such as index of overlap γ, PPM/OPPM's multiplicity M, will be presented.

In the threshold-based code acquisition system, "hit" is the event when the photon counts in the first slot is higher than a preset threshold, which is denoted as Th. Also let P_c be the probability of "hit," we have

$$P_c \equiv P_r\{Y_0 \geq Th\} = \sum_{i=Th}^{\infty} \mathrm{Pos}(i, E[Y_0]), \quad (18)$$

where, $E[Y_0]$ is as (10) with I_0 is also decided as (12). Using the similar approach that used to analyze the OPPM demodulator-based code acquisition system, we can compute the average value of $E\{N_{ACQ}\}$ for threshold-based code acquisition as (13) where the average of $E\{P_{FAi}\}$ and $E\{\frac{1}{P_D}\}$ over l_i are as follows.

$$E\{P_{FAi}\} \equiv E_{l_i}\{P_{FA}|l = l_i\} = \sum_{l=0}^{N-1} P_r\{l\} \sum_{i=Th}^{\infty} \mathrm{Pos}(i, (l+1)\lambda_s + \lambda_d), \quad (19)$$

$$E\left\{\frac{1}{P_D}\right\} \equiv E\left\{\frac{1}{P_D|l}\right\} = \sum_{l=0}^{N-1} P_r\{l\}\frac{1}{\sum_{i=Th}^{\infty} \mathrm{Pos}\left(i, \left(\frac{\omega}{2} + l\right)\lambda_s + \lambda_d\right)}. \quad (20)$$

Replacing (19) and (20) to (13), the average of $E\{N_{ACQ}\}$ for the threshold-based code acquisition can be computed.

4. Numerical Results

For the numerical calculation, a fixed OOC code length

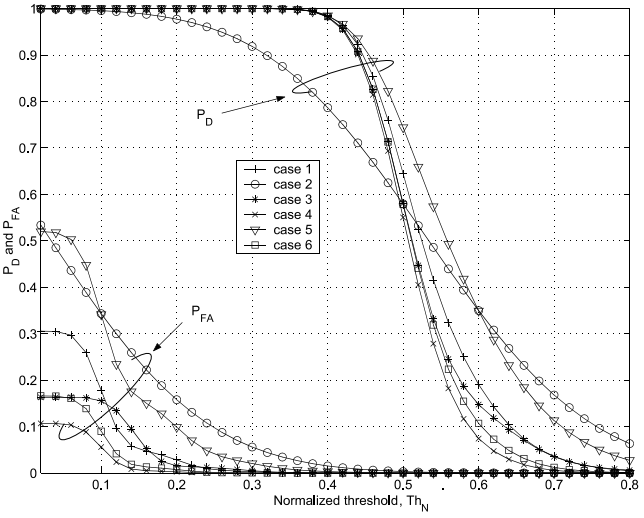

Fig. 6 Probability of false alarm and detection for different cases of $C \equiv \{\gamma, M, N, \omega, \lambda_d\}$; case 1: $C = \{16, 64, 30, 10, 0\}$, case 2: $C = \{16, 64, 30, 10, 1000\}$, case 3: $C = \{16, 64, 30, 7, 0\}$, case 4: $C = \{16, 64, 10, 10, 0\}$, case 5: $C = \{16, 32, 30, 10, 0\}$, case 6: $C = \{8, 64, 30, 10, 0\}$. Other parameters: $\mu = 50$, $K = 10$, and $L = 2000$.

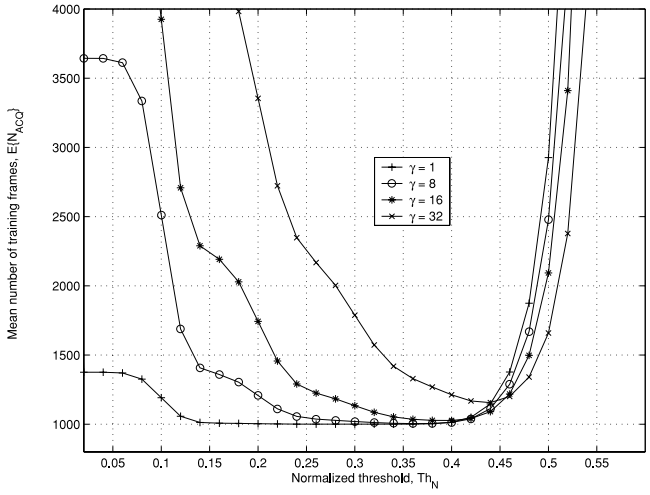

Fig. 7 Mean number of training frames versus normalized threshold Th_N for different γ. Threshold-based code acquisition with number of users $N = 50$, PPM/OPPM multiplicity $M = 64$, $\lambda_d = 0$, $K = 10$, average photon counts per information nat $\mu = 50$, OOC length $L = 2000$ and weight $\omega = 10$.

$L = 2000$ is used so as the number of states in Markov chain model is kept unchanged. The mean number of training frames is evaluated against normalized threshold (for threshold-based code acquisition system only) defined as $Th_N = \frac{Th - \lambda_d}{\omega \lambda_s}$, and average photon counts per information nat, μ, with which the average photon counts per code chip can be obtained as $\lambda_s = \frac{\mu \log M}{\omega}$.

4.1 Mean Number of Training Frames versus Normalized Threshold

From Figs. 7–11, we analyze the effects of index of overlap γ, PPM/OPPM multiplicity M, number of users N, OOC code weight ω and darkcurrents λ_d on the performance of threshold-based code acquisition versus normalized threshold. For this analysis, average photon counts per information nat $\mu = 50$ is selected, and number of penalty frames K is taken to be 10.

First, it is seen in these figures that there exists a range of optimal normalized threshold, where a mean number of training frames equivalent to a half code length, i.e. 1000 frames, is required to locate the correct cell. When normalized threshold is either decreased or increased outside this range, the mean number of training frames is exceedingly increased. The existence of this range of optimal threshold can be explained using Fig. 6 that shows P_{FA} and P_D versus normalized threshold Th_N. It is seen that when Th_N is at low level ($Th_N < 0.4$), $P_D \approx 1$ because photon counts over the first slot is always higher than threshold when the correct cell is observed. The increase of Th_N results in lower P_D because the possibility that photon counts over the first slot is higher than threshold is decreased with the higher threshold. Similarly, P_{FA} is also decreased as Th_N increases. However, as false alarm happens when an incorrect cell is observed, P_{FA} is at low level and is decreased quickly to 0 at low level of Th_N; for example at $Th_N = 0.15$ for case 4 in Fig. 6. Accordingly, there exists a range of Th_N where $P_D \approx 1$ and $P_{FA} \approx 0$. At this range, the optimal performance is achieved due to the nature of equation (13). Outside this range, either $P_D < 1$ or $P_{FA} > 0$ will result in the mean number of training frames higher than a half code length.

Furthermore, as also shown in Figs. 7–11, the range of optimal normalized threshold is depended on the selection of other system parameters. Following is our detail investigation. Note that in Fig. 6, we present six different cases of system parameter selections. By these selections, the trends of P_D and P_{FA} can be observed when one of five system parameters $(\gamma, M, N, \omega, \lambda_d)$ varies.

Figure 7 shows mean number of training frames versus normalized threshold for different γ. The number of users $N = 50$, PPM/OPPM multiplicity $M = 64$, $\lambda_d = 0$ are used. It is seen that the increase of γ degrades the code acquisition performance in the sense that the range of optimal normalized threshold becomes narrower. This is because higher γ results higher possibility of overlapping between users, i.e. higher MAI. Consequently, P_{FA} is increased as shown Fig. 6 (case 1 vs. case 6). Therefore, as Th_N decreases from 0.4, where $P_D \approx 1$, higher γ results in higher mean number of training frames. This makes the range of optimal normalized threshold narrower.

Figure 8 shows the mean number of training frames versus normalized threshold for different M. The number of users $N = 50$, index of overlap $\gamma = 8$, $\lambda_d = 0$ are used. It is seen that the increase of M improves the code acquisition performance as the range of optimal threshold becomes wider. Similar settings with $M = 64$ are also used for different number users N in Fig. 9. We also see the wider range of optimal threshold when the number of user decreases. Noting that lower M or higher N results in higher MAI, i.e.

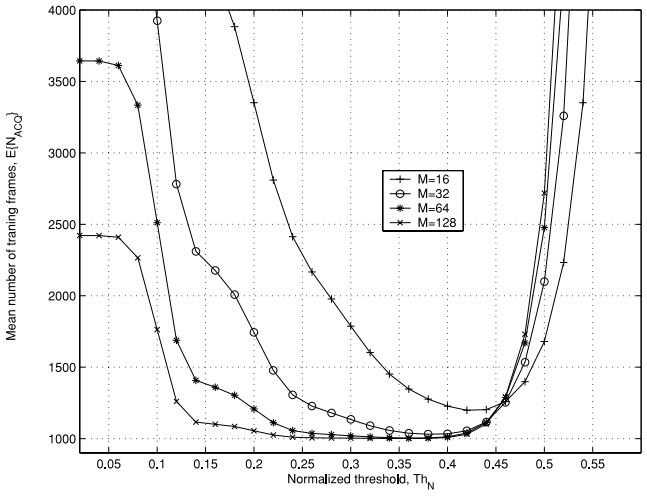

Fig. 8 Mean number of training frames versus normalized threshold Th_N for different PPM/OPPM multiplicity M. Threshold-based code acquisition with number of users $N = 50$, index of overlap $\gamma = 8$, $K = 10$, $\lambda_d = 0$, average photon counts per information nat $\mu = 50$, OOC length $L = 2000$ and weight $\omega = 10$.

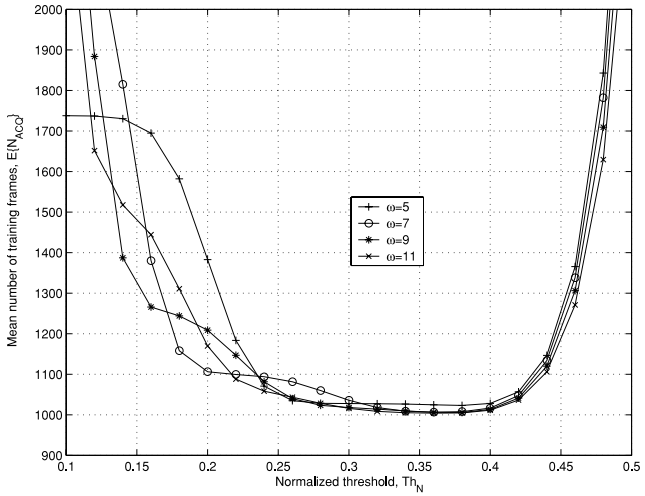

Fig. 10 Mean number of training frames versus normalized threshold Th_N for different ω. Threshold-based code acquisition with number of users $N = 50$, PPM/OPPM multiplicity $M = 64$, index of overlap $\gamma = 8$, $K = 10$, $\lambda_d = 0$, average photon counts per information nat $\mu = 50$, OOC length $L = 2000$.

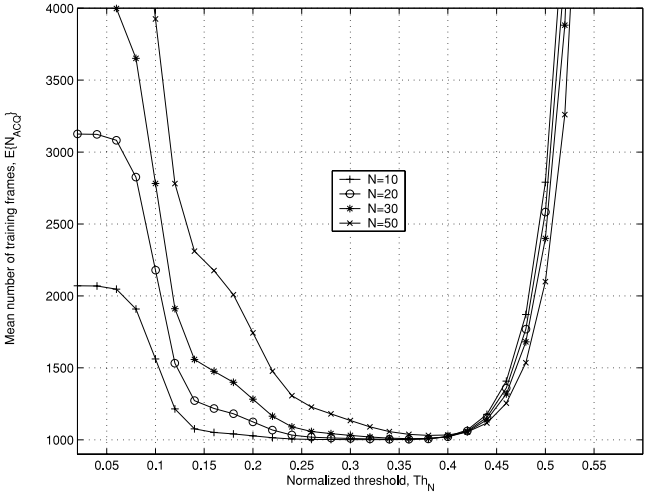

Fig. 9 Mean number of training frames versus normalized threshold Th_N for different number of users N. Threshold-based code acquisition with PPM/OPPM multiplicity $M = 64$, index of overlap $\gamma = 8$, $K = 10$, $\lambda_d = 0$, average photon counts per information nat $\mu = 50$, OOC length $L = 2000$ and weight $\omega = 10$.

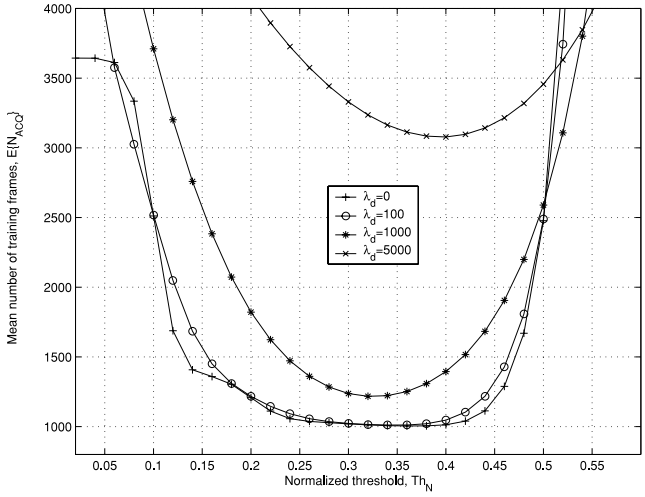

Fig. 11 Mean number of training frames versus normalized threshold Th_N for different λ_d. Threshold-based code acquisition with number of users $N = 50$, PPM/OPPM multiplicity $M = 64$, index of overlap $\gamma = 8$, $K = 10$, average photon counts per information nat $\mu = 50$, OOC length $L = 2000$ and weight $\omega = 10$.

higher P_{FA} (see Fig. 6, case 1 vs. case 5, and case 1 vs. case 4, respectively), these two arguments can also be explained similarly to that of Fig. 7.

In Fig. 10, the performance of threshold-base code acquisition is analyzed for different ω. Actually, higher ω results in higher number of interfering optical pulses. However, higher ω also causes higher threshold with a particular Th_N. Therefore, the change of ω does not affect much to P_{FA} at the optimal performance, as it is shown in Fig. 6 (case 1 vs. case 3). As a result, it is seen in Fig. 10 that the range of optimal normalized threshold is almost similar when ω varies. Actually, with normalize threshold $Th_N \in \{0.25 - 0.4\}$, similar performance of code acquisition system can be seen for $\omega = 5, 7, 9$, and 11.

Finally, Fig. 11 presents the effect of darkcurrents on the performance of threshold-based code acquisition versus normalized threshold. It is shown that darkcurrents degrade the system performance in terms of both optimal normalized threshold range and optimal performance itself. As λ_d increases, the range of optimal normalized threshold is decreased, and the required mean number of training frames increases significantly. For example, when $\lambda_d = 5000$, at least 3000 training frames are required to achieve the ACQ state, about 3 times higher than that of the case when $\lambda_d = 0$.

Actually, as it is seen in Fig. 6, when there is no darkcurrents ($\lambda_d = 0$), P_D can approach 1 when the normal-

ized threshold is at low level, and P_{FA} reaches 0 when the normalized threshold is high enough. Optimal performance exists where $P_D \approx 1$ and $P_{FA} \approx 0$; and mean number of training frames is as low as 1000. This scenario however does not happen in the presence of darkcurrents (case 2). At low normalized threshold, high darkcurrents overwhelm MAI that results in lower P_D. Since there are fewer optical pulses in the first slot when an incorrect cell is observed, high darkcurrents result in higher P_{FA} as it is shown in Fig. 6 (case 1 vs. case 2). As a result, the optimal performance in the presence of darkcurrents, which is resulted from $P_D < 1$ and $P_{FA} > 0$, is degraded.

4.2 Mean Number of Training Frames versus Average Photon Counts per Information Nat

In this section, we compare the performance of the two code acquisition schemes versus average photon counts per information nat μ for different index of overlap γ, multiplicity M, and darkcurrents λ_d. For this analysis, the OOC code weight $\omega = 10$ and the number of users $N = 50$ are used, the number of penalty frames K is also taken to be 10; for threshold-based code acquisition system, an optimal normalized threshold, $Th_N = 0.4$, is selected.

First, Figs. 12 and 13 present the mean number of training frames versus average photon counts per information nat with different γ. For this analysis, we use $M = 64$, and $\lambda_d = 0$. It is seen that when μ increases, while better performance can be achieved in the threshold-based code acquisition, the performance of demodulator-based code acquisition is degraded. Moreover, the threshold-based code acquisition offers much better performance, in terms of mean number of training frames, than the demodulator-based one does. Actually, when $\mu > 40$, which is considered the minimum requirement for the acceptable performance of OPPM fiber-optic CDMA systems [12], the demodulator-based code acquisition requires about 7 to 10 times more training frames than threshold-based one does.

In fact, for a fixed γ, the increase of μ results in higher P_D in both systems as photon counts over the first slot becomes higher. On the other hand, when μ increases in the threshold-based system, threshold becomes higher accordingly as Th_N is fixed. This results in lower P_{FA}. Meanwhile, when an incorrect cell is observed in the demodulator-based system, higher μ results in higher possibility that photon counts over some slot is higher than that of the first one. This causes higher P_{FA}. Consequently, we have results as mentioned.

Moreover, it is also seen that the effect of γ is different in two schemes. Actually, for a fixed μ, higher γ results in higher MAI in both systems. However, in the threshold-based code acquisition system, as the first slot is compared to the threshold lever to decide a "hit," P_{FA} and P_D become higher. In contrast, a "hit" is decided upon a comparison between the first slot and all the remaining ones. Therefore, higher MAI in all slots results in lower P_{FA} and P_D in the demodulator-based system. Noting because there

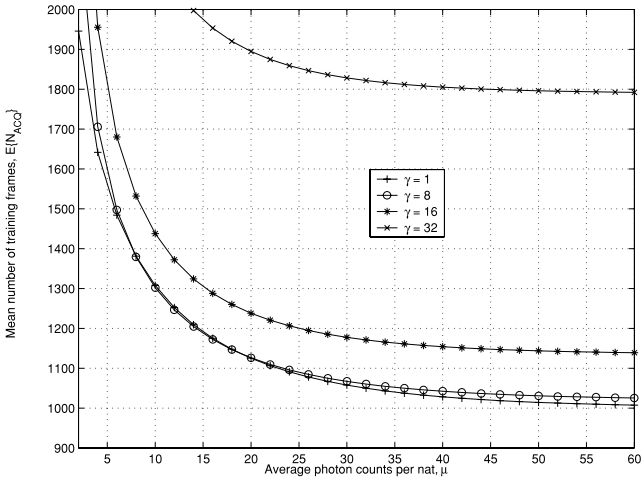

Fig. 12 Mean number of training frames versus average photon counts per information nat μ for different γ. Threshold-based code acquisition system with optimal normalized threshold $Th_N = 0.4$, number of users $N = 50$, PPM/OPPM multiplicity $M = 64$, $\lambda_d = 0$, $K = 10$, OOC's length $L = 2000$ and weight $\omega = 10$.

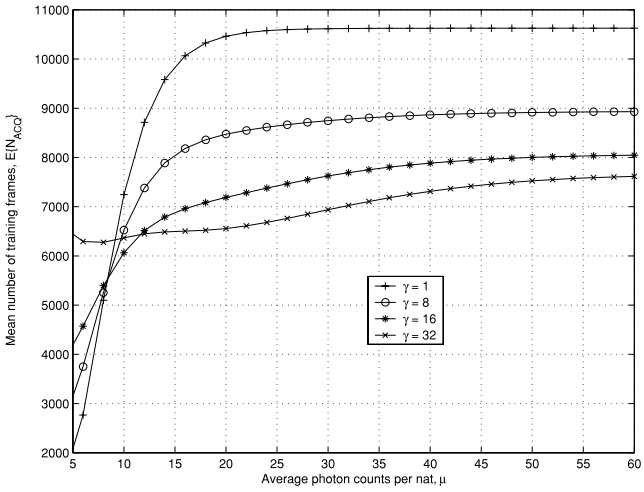

Fig. 13 Mean number of training frames versus average photon counts per information nat μ for different γ. Demodulator-based code acquisition with number of users $N = 50$, PPM/OPPM multiplicity $M = 64$, $\lambda_d = 0$, $K = 10$, OOC's length $L = 2000$ and weight $\omega = 10$.

will be fewer optical pulses in the slot 1 when an incorrect cell is observed, the effect of MAI on P_{FA} due to a change of γ is higher than that on P_D. Consequently, in the threshold-based code acquisition system, higher γ degrades the system performance. In contrast, the performance of the demodulator-based system is improved with higher γ.

Next, the comparison between the performance of two code acquisition schemes versus μ for different M is presented in Figs. 14 and 15. We use $\lambda_d = 0$, and $\gamma = 8$ for the analysis. It is seen that while the increase of μ improves the performance of threshold-based code acquisition system, it degrades the demodulator-based system. This argument can also be explained similarly as in Fig. 12 and 13. Moreover, effects of M in the two code acquisition systems are also

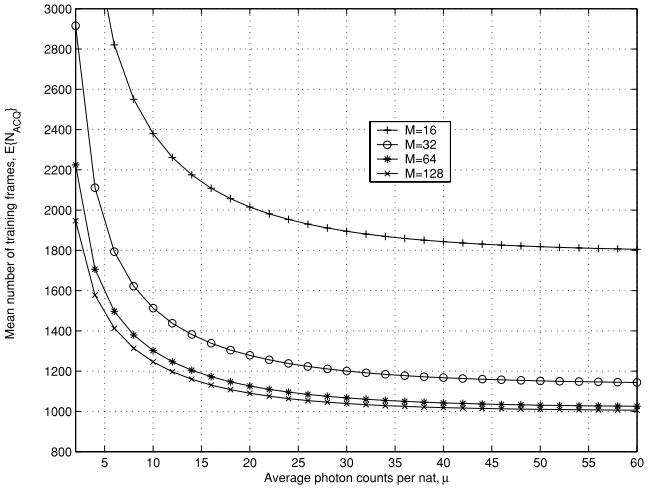

Fig. 14 Mean number of training frames versus average photon counts per information nat μ for differnt PPM/OPPM multiplicity M. Threshold-based code acquisition system with optimal normalized threshold Th_N = 0.4, number of users $N = 50$, index of overlap $\gamma = 8$, $\lambda_d = 0$, $K = 10$, OOC's length $L = 2000$ and weight $\omega = 10$.

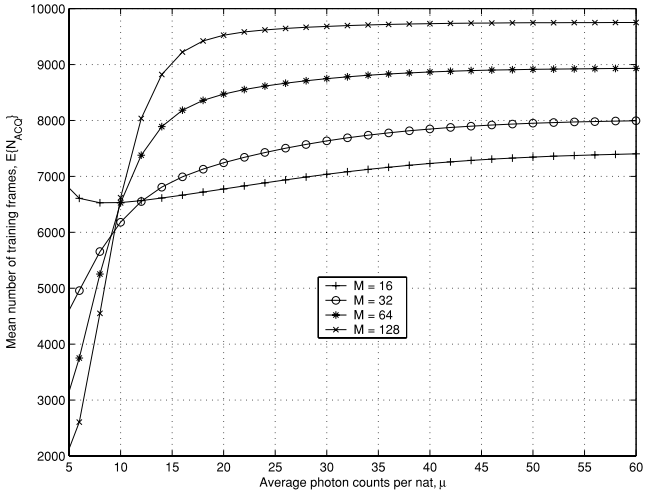

Fig. 15 Mean number of training frames versus μ for different PPM/OPPM multiplicity M. Demodulator-based code acquisition system with number of users $N = 50$, index of overlap $\gamma = 8$, $\lambda_d = 0$, $K = 10$, OOC's length $L = 2000$ and weight $\omega = 10$.

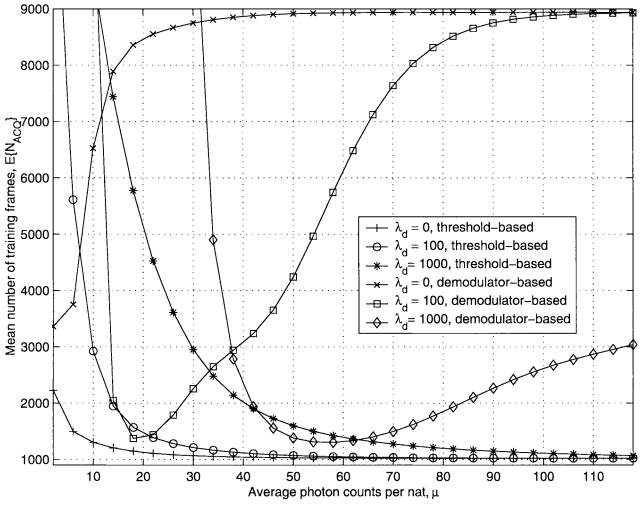

Fig. 16 Mean number of training frames versus average photon counts per information nat μ for different λ_d. Demodulator-based code acquisition versus threshold-based one with optimal normalized threshold $Th_N = 0.4$. Number of users $N = 50$, PPM/OPPM multiplicity $M = 64$, index of overlap $\gamma = 8$, $K = 10$, OOC's length $L = 2000$ and weight $\omega = 10$.

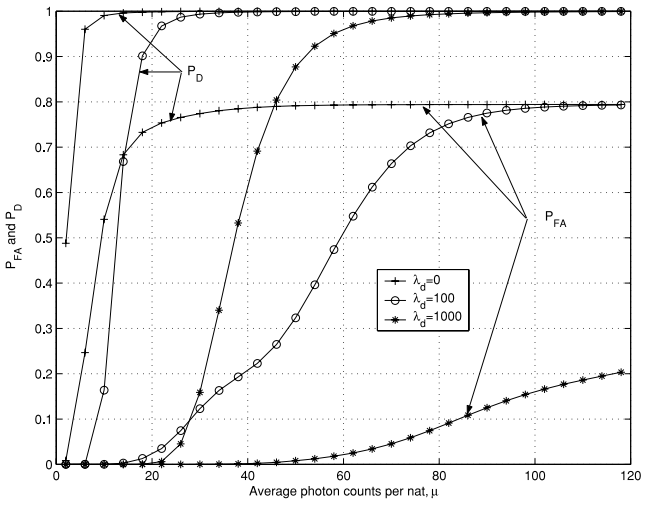

Fig. 17 Probability of false alarm and detection versus μ in demodulator-based code acquisition for different λ_d. Other parameters: similar to Fig. 16.

different. When M is increased in the threshold-based code acquisition system, interfering pulses are more distributed, i.e. lower MAI. We therefore have lower P_{FA} that results in better performance. On the other hand, with the same γ, higher M results in higher MAI in every slot. This results in higher P_{FA} in the demodulator-based system, i.e. system performance is degraded.

Finally, Fig. 16 shows the performance comparison of two schemes versus μ for different λ_d. For this analysis, we use $M = 64$, and $\gamma = 8$. It is seen that the increase of λ_d degrades the threshold-based code acquisition. However, when μ increases, mean number of training frames is continuously decreased. When μ is relatively high, effect of darkcurrents becomes minor because it is overwhelmed by MAI. As an optimal threshold is selected, the optimal performance therefore can be achieved when μ is high enough.

Nevertheless, the effect of λ_d is quite different in demodulator-based code acquisition. We investigate this with help of Fig. 17. It is seen that when μ becomes higher, both P_D and P_{FA} increase accordingly. When λ_d is small ($\lambda_d = 0$ for example), there is only effect of MAI; and P_D can quickly reach 1 as μ increases. However, as P_{FA} is also increased quickly, the mean number of training frames increases when μ increases. However, when λ_d becomes higher, higher μ is required so that MAI can overwhelm darkcurrents. When incorrect cell is observed, even higher μ is required because there are fewer optical pulses in the first slot. As a result, P_D is increased faster than P_{FA}, as it

is seen in Fig. 17. This situation results in the phenomenon that the mean number of training frames is first at high level, corresponding to both low P_D and P_{FA}. The mean number of training frames is then decreased because P_D is increased and P_{FA} is still at low level. When μ is high enough to overwhelm darkcurrents, P_{FA} starts increasing; and this results in the increase of the mean number of training frames, as shown in Fig. 16.

5. Conclusions

This paper has proposed and theoretically analyzed two code acquisition schemes for PPM/OPPM fiber-optic CDMA systems, namely threshold-based and demodulator-based code acquisition. The mean number of training frames is derived taking into account MAI, shot-noise and darkcurrents.

It is shown that optimal performance of threshold-based code acquisition system is sensitive to normalized threshold. The range of optimal normalized threshold is decided upon the selection of system settings, however, normalized threshold should not be less than 0.15 or higher than 0.4. While higher index of overlap or higher number of users results in narrower the range of optimal normalized threshold, the increase of multiplicity widens this range. The change of code weight does not affect much to the range of optimal normalized threshold whereas the increase of darkcurrents significantly degrades threshold-based code acquisition both in terms of range of optimal normalized threshold and optimal performance. Notably, when normalized threshold is properly selected, it is shown that the threshold-based code acquisition system offers much better performance than demodulator-based one.

Acknowledgement

The authors would like to thank the reviewers for their thorough reviews and useful suggestions for improving the readability of this paper.

References

[1] A. Stok and E.H. Sargent, "Lighting the local area optical code-division multiple access and quality of service provisioning," IEEE Network, vol.14, no.6, pp.42–46, Nov./Dec. 2000.
[2] A. Stok and E.H. Sargent, "The role of optical CDMA in access networks," IEEE Commun. Mag., vol.40, no.9, pp.83–87, Sept. 2002.
[3] J.A. Salehi, "Code division multiple-access techniques in optical fiber networks—Part I: Fundamental principles," IEEE Trans. Commun., vol.37, no.8, pp.824–833, 1989.
[4] G.-C. Yang, "Performance analysis for synchronization and system on CDMA optical fiber networks," IEICE Trans. Commun., vol.E77-B, no.10, pp.1238–1248, Oct. 1994.
[5] M.M. Mustaphan and R.F. Ormondroyd, "Effect of multiaccess interference on code synchronization using a sequential detector in an optical CDMA LAN," IEEE Photonics Technol. Lett., vol.12, no.8, pp.1103–1105, 2000.
[6] M.M. Mustaphan and R.F. Ormondroyd, "Dual-threshold sequential detection code synchronization for an optical CDMA network in the presence of multi-user interference," IEEE J. Lightwave Technol., vol.18, no.12, pp.1742–1748, 2000.
[7] A. Keshsvatzian and J.A. Salehi, "Optical orthogonal code acquisition in fiber-optic CDMA systems via the simple serial-search method," IEEE Trans. Commun., vol.50, no.3, pp.473–483, 2002.
[8] A.T. Pham and H. Yashima, "Code acquisition with search/lock strategy in optical orthogonal CDMA systems," Proc. IASTED 2nd International Conference on Communication Systems and Networks, pp.412–417, 2003.
[9] K. Sato, T. Ohtsuki, H. Uehara, and I. Sasase, "Effect of imperfect slot synchronization on direct-detection optical synchronous CDMA communication systems with PPM signaling," IEEE J. Lightwave Technol., vol.14, no.9, pp.1963–1969, 1996.
[10] A.T. Pham and H. Yashima, "Overlapping pulse-position modulation fiber-optic CDMA systems impaired by imperfect synchronization," Proc. 2004 International Technical Conference on Circuits/Systems, Computers and Communications, pp.6F1L-1-1–6F1L-1-4, 2004.
[11] H.M.H. Shalaby, "Performance analysis of optical synchronous CDMA communication systems with PPM signaling," IEEE Trans. Commun., vol.43, no.2/3/4, pp.624–634, 1995.
[12] H.M.H. Shalaby, "A performance analysis of optical overlapping PPM-CDMA communication systems," IEEE J. Lightwave Technol., vol.17, no.3, pp.426–433, 1999.
[13] A. Polydoros and C.L. Weber, "A unified approach to serial search spread-spectrum code acquisition—Part I: General theory," IEEE Trans. Commun., vol.COM-32, no.5, pp.542–549, 1984.
[14] M.K. Simon, J.K. Omura, R.A. Scholtz, and B.K. Levitt, Spread spectrum communications handbook, revised version, McGraw-Hill, 1994.

Anh T. Pham was born in Thanh Hoa, Vietnam, in 1975. He received the B.E. and M.E. in electrical engineering degrees from Hanoi University of Technology, Hanoi, Vietnam, in 1997 and 2000 respectively. He is currently working towards a Ph.D. degree in Information and Computer Sciences at the Saitama University, Saitama, Japan. From 1998 to 2002, he was with NTT in Vietnam, where he worked as a network-planning engineer. His present research interests are in the area of spread spectrum technique and optical communications. Pham receives Japanese government scholarship (MonbuKagaku-sho) for his Ph.D. study. He also received Vietnamese government scholarship for undergraduate study.

Hiroyuki Yashima was born in Mie, Japan, in 1958. He received the B.E., M.E., and Ph.D. degrees from Keio University, Japan, in 1981, 1987, and 1990, respectively, all in electrical engineering. From 1990 to 2003, he was a Associate Professor at the Department of Information and Computer Sciences, Saitama University, Saitama, Japan. From 1994 to 1995, he was a Visiting Scholar at the University of Victoria, Victoria, British Columbia, Canada. His research interests include modulation and coding, optical communication systems, satellite communication systems, and spread spectrum communication systems. In 2003, he joined the Tokyo University of Science, Tokyo, Japan, as Professor at the Department of Management Science. Dr. Yashima received the 1989 Society of Satellite Professionals International Scholarship Award.